THE JOURNAL OF PHYSICAL CHEMISTRY A

Article

Cite This: J. Phys. Chem. A 2019, 123, 8562−8570

pubs.acs.org/JPCA

Vibrational Autodetachment from Anionic Nitroalkane Chains: From Molecular Signatures to Thermionic Emission

Christopher L. Adams,[†] Klavs Hansen,*[,‡,§] and J. Mathias Weber*[,†]

[†]JILA and Department of Chemistry, University of Colorado, Boulder, Colorado 80309-0440, United States

[‡]Center for Joint Quantum Studies and Department of Physics, School of Science, Tianjin University, 300072 Tianjin, P. R. China

[§]Department of Physics, Gothenburg University, SE-405 30 Gothenburg, Sweden

Supporting Information

ABSTRACT: We report the kinetic energy distributions in electron autodetachment from nitroethane, 1-nitropropane, and 1-nitrobutane anions upon laser excitation of CH stretching modes measured using velocity map electron imaging. In striking contrast to the case of nitromethane, the kinetic energy distributions show almost no distinct vibrational features, and they can be described by thermionic emission, relating the shape of the distributions to the electron capture cross section of the neutral molecule. The data suggest that a classical description is warranted above ca. 20 meV electron kinetic energy. At lower energies, quantum effects suppress the attachment cross section.

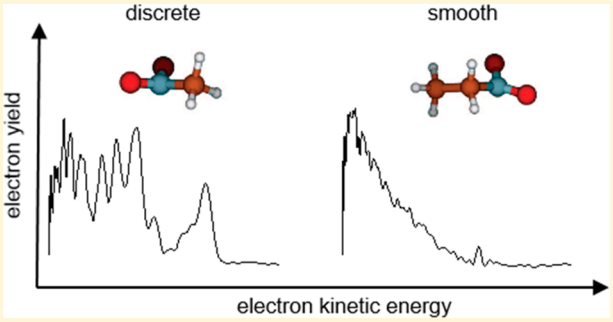

1. INTRODUCTION

The emission of particles from thermally excited physical systems is a commonly observed phenomenon. These processes can be divided into two classes, according to whether they involve only few quantum states or whether they can best be described in terms of thermal processes. Evaporative cooling is important in all size and temperature regimes, from macroscopic bodies (including our own) to molecular clusters, trapped atoms on their way to forming a quantum condensate, and excited nuclei. Similarly, electrons can be emitted from hot macroscopic metals (as described by the Richardson equation[1]), clusters,[2] and molecules.[3−7] More recently, also thermal photon emission has been observed from small carbon clusters.[8]

However, the delineation between the two regimes of direct versus thermal emission is not yet well established, in particular for electron emission, although this is of obvious interest for the description of the dynamics of molecules and clusters after photon absorption. Molecular anions provide a particularly convenient platform for the study of such electron emission processes because the excitation energies required for electron emission are relatively small, and a judicious choice of the molecular system can render other relaxation mechanisms inactive (e.g., dissociation).

In vibrational autodetachment (VAD) from small molecular systems, the kinetic energy distribution of the emitted electrons will carry signatures of the process as well as the molecular details of the molecule, such as the vibrational states, potentially for both of its neutral and ionic states. The theoretical foundations of the description of VAD were developed by Simons and co-workers,[7,9] following early experiments by the Brauman[10−13] and Beauchamp[14−16] groups based on work on highly excited anions. Spectroscopic studies based on VAD were later performed by several groups.[6,17−34]

A complete description of the emission process requires detailed knowledge of the vibrational states and the multidimensional potential energy surfaces of both the anion and the neutral, including the photon absorption process and the level and intersystem crossing dynamics. This poses a difficult theoretical and computational problem, and the description of the emission process will depend on the details of the system. However, the molecular signatures in the kinetic energy distribution broaden with increasing size of the system, and this suggests the possibility of a description of the emission processes with statistical approaches, which require less molecular level detail.[5,35,36]

In the present work, we systematically explore the evolution of the kinetic energy distribution of electrons emitted in vibrational autodetachment processes (VAD-KEDs) with the size of the molecular system, focusing on nitroalkane anions. These molecules are simple hydrocarbon chains with a CH_3 group on one end and an NO_2^- group on the other, the latter carrying most of the excess negative charge. The neutral molecules have all similar adiabatic electron affinities (AEA = 172−240 meV),[37−39] dipole moments (μ = (1.13−1.22) × 10^{-29} C·m),[40−42] and polarizabilities (α = (9.5−11.6) × 10^{-40} F·m^2).[41] They only vary in the number of CH_2 units between the terminal groups, which of course changes their vibrational spectra and their density of vibrational states. The nonresonant photoelectron spectra and vibrational spectra of the anions in

Received: August 14, 2019
Revised: September 17, 2019
Published: September 18, 2019

DOI: 10.1021/acs.jpca.9b07780
J. Phys. Chem. A 2019, 123, 8562−8570

the mid-infrared show well-resolved vibrational features that have been characterized in detail.[19,27,37−39] In nitroalkane anions, the vibrations of the NO_2^- group, most importantly the nitro wagging mode, play an important role in VAD. This mode most directly connects the potential energy surfaces of the negative ion and the neutral, as sufficient excitation in this mode allows the anion to explore geometries very close to the equilibrium geometry of the neutral, providing access to the electron emission channel.[6] In the description used below, where the cross section for the inverse process, electron attachment, plays a pivotal role, this can be translated into an efficient capture of the electron in the attachment process, mediated by subsequent energy dissipation into vibrational excitations.

We measured the VAD-KEDs of nitroethane, 1-nitropropane, and 1-nitrobutane anions upon infrared excitation of specific CH stretching vibrational modes using velocity-map photoelectron imaging. While the VAD-KED of nitromethane[38] shows clearly resolvable vibrational signatures, and even reflects the nature of the initially excited vibrational state, we show here that nearly no vibrational details are observable for any of the other nitroalkanes. We describe the VAD-KEDs through a statistical thermionic emission process and calculate the emission characteristics with a detailed balance approach.

2. EXPERIMENTAL SECTION

The experimental setup has been previously described in detail,[38] and only a brief summary will be given here. We entrained vapor of nitroalkanes, $CH_3(CH_2)_nNO_2^-$ (n = 1−3 for nitroethane, 1-nitropropane, and 1-nitrobutane, respectively), at room temperature into a pulsed supersonic expansion of argon. A counterpropagating electron beam created an electron impact ionization plasma in the high-density region of the expansion, forming the corresponding nitroalkane anions by attachment of slow, secondary electrons to the neutral precursor molecules, which were subsequently cooled during the expansion. On the basis of previous photoelectron spectroscopy experiments[38,39] on nitromethane and nitroethane, using the same instrument with similar source conditions, we take the effective vibrational ion temperature to be ca. 250 K. The anions were mass selected in a time-of-flight mass spectrometer and injected into the photodetachment region of a velocity-map photoelectron imaging spectrometer.

Photodetachment was performed with pulsed, linearly polarized, weakly focused, tunable radiation in the mid-infrared, generated by a Nd:YAG pumped optical parametric converter system. Pulse energies were several millijoules, with a bandwidth of ca. 2 cm^{-1}. Photoelectrons were accelerated perpendicular to the plane defined by the ion and laser beams into a field-free, double μ-metal shielded flight tube, and velocity mapped onto a dual microchannel plate detector coupled to a phosphor screen. The laser polarization was parallel to both the ion beam and the position sensitive electron detector of the velocity-map imaging spectrometer. The signal from the phosphor screen was sampled by using a CCD camera, centroided in real time (WENIMAGING program[43]), and several 10^6 photoelectron counts were accumulated for each image. The resulting photoelectron images were converted with an inverse Abel transformation (BASEX program[44]) to obtain an equatorial slice through the original three-dimensional velocity distribution. The transformed images were integrated over all emission angles at each radius to yield a photoelectron spectrum in velocity space, which was subsequently transformed into a spectrum as a function of electron kinetic energy. The spectra were calibrated to the well-known transitions in the photoelectron spectrum of S^- at 2.331 eV, taken with the second harmonic of a Nd:YAG laser. The experimental velocity resolution of the photoelectron imaging spectrometer was ca. 5000 m/s, corresponding to 5.3 meV at 100 meV kinetic energy.

The photoelectron spectra contain contributions from VAD as well as from direct detachment. As previously published spectra of nitroalkane anions show,[6,19,25,27,37−39] resonances from VAD are superimposed on a largely flat background from direct detachment. Similar to earlier work on VAD from nitromethane,[6] we obtained the VAD portion of the KEDs by subtracting the known photoelectron spectrum for each ion species,[37,39] properly weighing the relative intensities of the direct and VAD channels, and correcting for threshold effects by using a threshold law previously applied to work on nitromethane.[6,38] The resulting KEDs shown in the present work can be considered to be purely due to VAD.

3. THEORY

The spectra of electrons thermally emitted from molecular anions can be calculated by detailed balance considerations[5,45] as

$$P(E)\,\mathrm{d}E \propto \sigma(E) E \mathrm{e}^{-E/k_\mathrm{B}T}\,\mathrm{d}E \tag{1}$$

where E is the measured kinetic energy of the emitted electron, σ is the angle-averaged capture cross section for the inverse process (i.e., electron attachment), and T is the (microcanonical) temperature of the neutral product molecule after electron emission. The microcanonical temperature is defined with an expansion of the logarithm of the total vibrational level density of the product, $\rho(E)$, at the neutral product molecule excitation energy:[46]

$$\frac{1}{k_\mathrm{B}T} \equiv \frac{\mathrm{d}[\ln \rho(E)]}{\mathrm{d}E} \tag{2}$$

In this work, the temperature will be kept as a fit parameter, and the main unknown at this point is the capture cross section, σ. No experimental data exist for low-energy electron attachment to any of the species under study here that have sufficient energy resolution (a few tens of meV or better), so these cross sections have to be modeled. In the remainder of this section, we will summarize how the capture cross section can be treated in terms of quantum mechanical, classical, and empirical scattering models.

In general terms, the Hamiltonian governing the electron−molecule interaction for a point-like molecule with polarizability α and permanent dipole moment $\vec{\mu}$ can be written as

$$\hat{H} = \frac{\hat{\vec{p}}^{\,2}}{2m_\mathrm{e}} + \frac{\mu e \cos\theta}{4\pi\epsilon_0 r^2} - \frac{e^2\alpha}{2(4\pi\epsilon_0)^2 r^4} \tag{3}$$

where μ is the magnitude of the dipole moment, r is the electron−molecule distance, and θ is the angle between the direction of the dipole moment and the vector from the molecule to the electron. Quantum mechanically, the limiting behavior of electron attachment for small kinetic energies and in the absence of a permanent dipole moment is given by Wigner's threshold laws[47,48] as

$$\sigma(E) \propto E^{l-1/2} \tag{4}$$

DOI: 10.1021/acs.jpca.9b07780
J. Phys. Chem. A 2019, 123, 8562−8570

where l is the angular momentum of the free electron, and the electron−molecule interaction potential must decay faster than $1/r^2$. For most molecules, electron attachment at low energies is predominantly an s-wave process, so $\sigma(E) \propto E^{-1/2}$. However, this limiting behavior is strictly only correct at threshold, and the attachment cross section is often observed to fall off more rapidly at energies as low as 1 meV, also in the absence of a permanent dipole moment.[49−57]

As mentioned above, the long-range electron-dipole interaction potential ($\propto 1/r^2$) does not decrease sufficiently fast for large r for Wigner's threshold laws to be valid. All molecules in the present work have strong dipole moments, which are even above the limit for forming dipole-bound states. This limit is 5.42×10^{-30} C·m for nonrotating dipoles[58] and in practical cases takes values above ca. 6.7×10^{-30} C·m.[59] Dipole-bound states have in fact been observed in photoelectron spectroscopy imaging experiments on nitromethane and nitroethane.[38,39] While a quantum theory for the capture of an electron by a stationary dipolar molecule has been formulated by Troe and co-workers,[60,61] the theory gives thermally averaged attachment rates and does not lend itself to a simple analytical expression for the attachment cross section as a function of electron kinetic energy; its application is therefore beyond the scope of the current work. However, electron capture by dipolar molecules can be treated using an empirical approach based on limiting behavior. While the Wigner threshold law does not hold strictly for the electron-dipole potential ($\propto 1/r^2$), this potential decays faster than the attractive Coulomb potential ($\propto 1/r$), where the capture cross section is proportional to $1/E$.[48] As proposed by Klots[62] and shown experimentally by Hotop and co-workers,[52−57] the capture cross section for many molecules can be described with a behavior between Wigner's threshold law for s-wave capture ($\propto 1/E^{1/2}$) and the behavior for attractive Coulomb potentials ($\propto 1/E$).

The attachment process can also be modeled classically. For an electron impinging on a stationary point-like molecule without permanent dipole moment, where the electron−molecule interaction is given by an induced-dipole potential, the capture cross section is represented by Vogt−Wannier theory (for which the classical version is the Langevin cross section). The cross section obtained this way is proportional to $E^{-1/2}$,[5,45,46,63,64] consistent with the quantum mechanical treatment of s-wave capture, except for a factor of 2 in absolute cross section at low energies. Fabrikant and Hotop[49] extended Vogt−Wannier theory to include dipole moments up to the critical dipole moment that can support a dipole-bound state. Because the molecules studied in the present work all have dipole moments far in excess of this critical dipole, we will use a flexible model instead, which we will call the modified Langevin model and which can be realized by using the expression

$$P(E)\,\mathrm{d}E \propto E^{\gamma} \mathrm{e}^{-E/k_{\mathrm{B}}T}\,\mathrm{d}E \tag{5}$$

The parameter $\gamma = 1/2$ represents the limit of Langevin (or Wigner s-wave) capture but will be a fit parameter for the present work. In the context of an empirical model based on limiting behavior between short-range s-wave capture and Coulomb capture as discussed above, the other limiting case would be $\gamma = 0$ for a $1/E$ dependence of the cross section. Hotop and co-workers have used a similar expression to describe low-energy electron attachment.[52−57]

In a recent paper,[65] Hansen extended the classical electron capture treatment to include a stationary point dipole. Similar to the original Langevin treatment, the energy-dependent attachment cross section was calculated by locating the limiting impact parameter b_c for which trajectories do not have a turning point in the radial motion. For a physical picture, the repulsive end of the dipole moment prevents the electron from getting into the region where the polarizability potential causes irreversible "spiraling" into the molecule. This translates to a critical energy, below which no capture takes place for certain orientations of the dipole relative to the electron's direction of approach.

We will extend this to a calculation of the classical cross section of a finite size molecule with the expectation that it will represent the experimental data at high energies. Following the procedure given in ref 65, the classical version of the Hamiltonian in eq 3 is solved to establish the condition obeyed at the turning point, r_t, of the radial motion:

$$\frac{1}{r_t^{\,2}} = \frac{E\left(b^2 + \frac{\mu e \cos\theta}{E4\pi\epsilon_0}\right)}{\frac{e^2\alpha}{(4\pi\epsilon_0)^2}}\left(1 - \sqrt{1 - \frac{\frac{2e^2\alpha}{(4\pi\epsilon_0)^2}}{E\left(b^2 + \frac{\mu e \cos\theta}{E4\pi\epsilon_0}\right)^2}}\right) \tag{6}$$

This expression must be real and positive to have a physically meaningful turning point. If the finite capture radius is disregarded, the cross section is given as $\sigma = \pi b_c^{\,2}$, where b_c is the largest impact parameter that does not cause r_t to be imaginary. This yields the capture cross section

$$\sigma(E, \theta) = \pi b_c^{\,2} = \pi\left(\left(\frac{2e^2\alpha}{E(4\pi\epsilon_0)^2}\right)^{1/2} - \frac{\mu e \cos\theta}{E4\pi\epsilon_0}\right) \tag{7}$$

for

$$E^{1/2} \geq \frac{\mu \cos\theta}{\sqrt{2\alpha}} \tag{8}$$

For sufficiently high energy, the critical turning point in the radial motion will be inside the molecule. For these situations, the finite capture radius, r_m, can be taken into account, which acts as a "black hole" radius for capturing the electron with unit probability. We will call the model based on this physical situation the finite size dipole model. We first determine the energies where this occurs. For given E and θ, the value of r_t^{-2} decreases with increasing b^2; i.e., the radius of the turning point increases with the impact parameter b, as expected. The cross section is therefore found by inserting the critical value b_c in eq 7 into eq 6 with $r_t = r_m$. Solving for the energy gives the dividing line between the low- and the high-energy regimes as

$$E_c = \frac{1}{2r_m^{\,4}}\frac{e^2\alpha}{(4\pi\epsilon_0)^2} \tag{9}$$

Above this energy, the cross section is found by solving for the critical impact parameter where $r_t = r_m$, yielding

$$\sigma(E, \theta) = \pi b_c^{\,2} = \pi\left(r_m^{\,2} + \frac{e^2\alpha}{2Er_m^{\,2}(4\pi\epsilon_0)^2} - \frac{\mu e \cos\theta}{E4\pi\epsilon_0}\right) \tag{10}$$

To make numerical estimates, a meaningful value of r_m must be inserted. The molecular size is extrapolated from bulk densities with the equation representing the spherical approximation

DOI: 10.1021/acs.jpca.9b07780
J. Phys. Chem. A 2019, 123, 8562−8570

$$r_m = \left(\frac{3v}{4\pi}\right)^{1/3} \tag{11}$$

where v is the molecular volume given by the bulk density. The molecular parameters for the molecules under study are given in Table 1. The total cross sections are calculated with an integration over θ:

Table 1. Selected Properties of Nitroethane, Nitropropane, and Nitrobutane

molecule	μ^a (10^{-29} C·m)	α^a (10^{-40} F·m^2)	bulk density (g/cm)^3	r_m (Å)	AEA (meV)
nitroethane	1.13	10.7	1.05	3.05	191[b]
nitropropane	1.22	9.46	1.00	3.28	223[c]
nitrobutane	1.13	11.6	0.973	3.48	240[d]

[a]From refs 40−42. [b]From ref 39. [c]From ref 37. [d]From ref 37.

$$\sigma(E) = \frac{1}{2}\int_{\theta_0}^{\pi} \sin\theta\sigma(E,\theta)\,d\theta \tag{12}$$

where the azimuthal angle has already been integrated out. The value θ_0 is determined from eq 8. The result is the cross section

$$\sigma(E) = \pi\left(r_m^2 + \frac{e^2\alpha}{2Er_m^2(4\pi\epsilon_0)^2}\right) \tag{13}$$

for

$$E \geq \frac{1}{2r_m^4}\frac{e^2\alpha}{(4\pi\epsilon_0)^2} \tag{14}$$

Overall, our treatment results in three regions of the (θ, E) plane, shown in Figure 1. The cross-section behavior is thus divided into three parts, depending on the electron kinetic energy E. The high-energy part is given by eqs 13 and 14. For lower energies, the cross section has been determined previously[65] by using the definition

$$E_0 = \frac{\mu^2}{2\alpha} \tag{15}$$

as

$$\sigma(E) = \pi\left(\frac{2e^2\alpha}{E(4\pi\epsilon_0)^2}\right)^{1/2} \quad \text{for } E_0 \leq E \leq \frac{1}{2r_m^4}\frac{e^2\alpha}{(4\pi\epsilon_0)^2} \tag{16}$$

and

$$\sigma(E) = \pi\left(\frac{2e^2\alpha}{E(4\pi\epsilon_0)^2}\right)^{1/2}\left(1 + \frac{1}{4}\left(\sqrt{\frac{E_0}{E}} - \sqrt{\frac{E}{E_0}}\right)\right) \quad \text{for } E \leq E_0 \tag{17}$$

4. RESULTS AND DISCUSSION

Figure 2 shows the experimental VAD-KEDs of nitroalkane anions, $CH_3(CH_2)_nNO_2^-$ for n = 0−3, generated upon excitation of the lowest energy CH stretching vibration for each species. The vibrational modes in these examples are

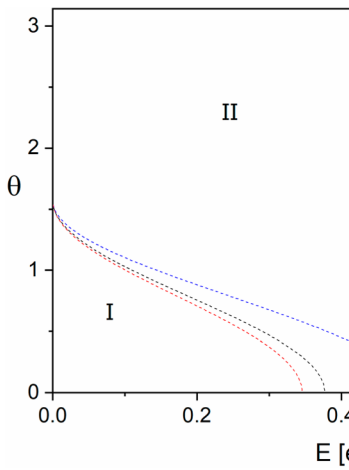

Figure 1. Different trajectory regions for the cross sections for nitroethane (black), nitropropane (blue), and nitrobutane (red), with the parameters given in Table 1. In region I (left/below the dotted lines), no capture occurs, in region II (between the dotted lines and the vertical lines) the low-energy eq 7 holds, and in region III (to the right of the vertical lines) eq 13 holds.

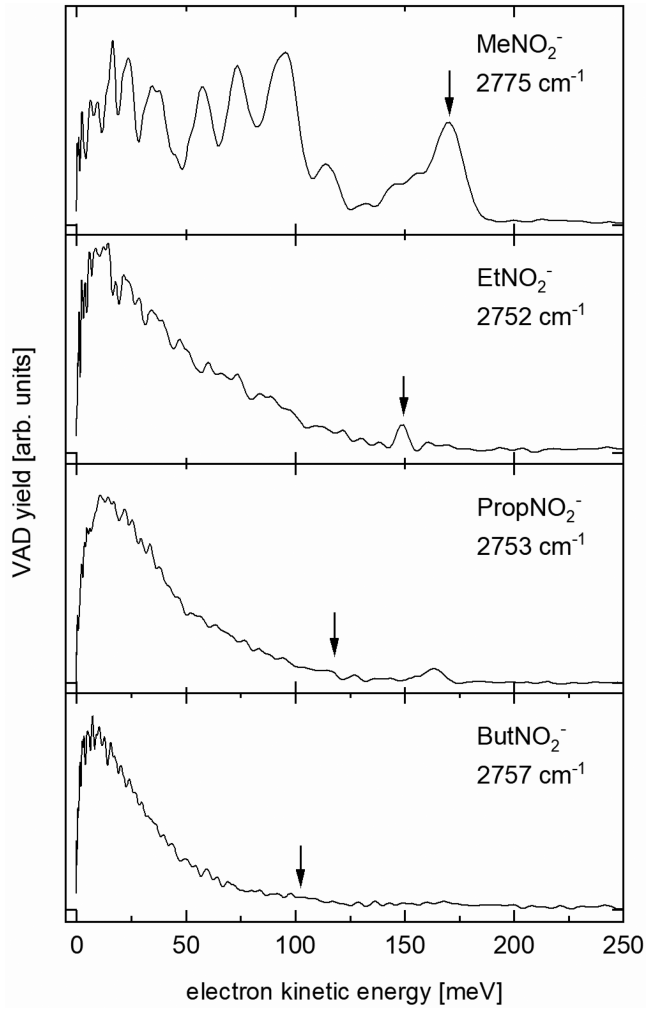

Figure 2. Experimental VAD-KEDs of nitroalkane anions, $CH_3(CH_2)_nNO_2^-$ for n = 0−3 (top to bottom), generated upon excitation of the lowest energy CH stretching vibration for each species. Excitation wavenumbers are noted for each species. The data for nitromethane were taken from ref 6. The arrows on each trace indicate the expected position of the 0 → 0 band.

DOI: 10.1021/acs.jpca.9b07780
J. Phys. Chem. A 2019, 123, 8562−8570

similar in that they involve mainly the motion of the CH oscillator closest to the nitro group, whose CH stretching frequency is strongly red-shifted from typical CH stretching frequencies in neutral nitroalkanes, due to negative hyperconjugation effects.[66] The excitation energies are also very similar, in particular those for nitroethane, nitropropane, and nitrobutane (n = 1−3), within 5 cm^{-1} of each other. The VAD-KED of nitromethane anion (n = 0) exhibits pronounced vibrational structure, which has been described in detail in earlier work,[6] based on the density of vibrational final states in the neutral nitromethane molecule formed by VAD. In striking contrast, all other nitroalkane anions have largely featureless VAD-KEDs. The small peak at ca. 150 meV in the VAD spectrum of nitroethane is consistent with the signature of the transition from the ground state of the anion to the ground state of the neutral. The similarly small peak at 163 meV in the VAD spectrum of nitropropane is most likely due to a vibrational Feshbach resonance.[37] These peaks are not part of the statistical emission model used here, and their intensity is a qualitative measure of how complete the energy randomization in the molecule is prior to electron emission. They become consistently less pronounced with increasing molecule size, suggesting that the excitation energy becomes better randomized the larger the molecule is.

The nearly complete loss of vibrational structure in the VAD-KEDs suggests that most molecular details are lost already upon the addition of a single CH_2 link in the nitroalkane chain. As a result, the VAD process can be well described by a statistical model, without the need to take into account the detailed vibrational spectrum of each target system. The small molecular size at which this onset of statistical behavior occurs and the abruptness of the loss of vibrational structure are quite striking. Going from nitromethane to nitroethane adds nine vibrational modes to the molecule, and several of these modes correspond to low-energy motions such as torsional modes or bending vibrations. This increases the density of vibrational states significantly, and we tentatively attribute the loss of vibrational features to a more efficient randomization of energy due to the increased density of states.

All the nitroalkane molecules investigated here have comparable dipole moments (ca. 1.16×10^{-29} C·m or 3.5 D) and static polarizabilities (ca. 10^{-39} F·m^2 or ca. 10^{-23} cm^3), governing the long-range behavior of the electron−molecule interaction. The dipole moments are of particular interest here, since they are sufficiently large to support a dipole-bound anion state, which—as mentioned—has been experimentally observed for nitroethane and nitromethane.[38,39] This suggests that the dipole moments should be taken into account for the description of the attachment cross section, which enters into the detailed balance model as the inverse process of electron emission.

Figure 3 shows the experimental data for excitations on the lowest energy vibrational modes compared with the models discussed above. While the classical models used here can represent the experimental data very well for energies above ca. 20 meV, they do not fit the experimental data for lower energies, regardless of the parameters used. As a result, the modified Langevin model was fitted to the whole energy range, while the fits of the temperature with the classical dipole polarizability calculation were made for energies above 20 meV. In all cases, the best curves for the point dipole model are nearly indistinguishable from those with a finite capture radius,

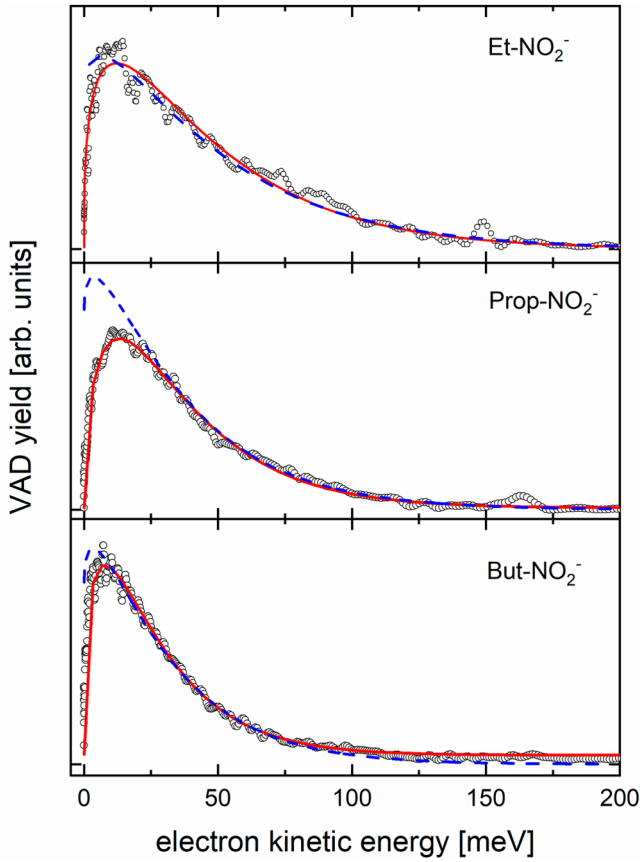

Figure 3. Comparison of the experimental VAD-KEDs after excitation of the lowest energy vibrational CH stretching mode (open circles) with the modified Langevin model (red solid line) and the classical dipole models (dashed blue line, the curves for the two versions are nearly identical). The modified Langevin model directly shows the nonlinear fit to the experimental data, while the fits of the temperature with the classical dipole polarizability calculation were made for energies above 20 meV.

and the temperatures of the neutral product molecule are only slightly different for the two models. We conclude from this observation that the model including the finite capture radius is not very sensitive to this parameter, at least not for the relatively low energies and temperatures that are involved in the present work. Model parameters for all molecules, excitation energies, and models are collected in Table 2.

The modified Langevin model (using a nonlinear fit with eq 5) gives a very good representation of the experimental data. Both of the classical dipole models, where the effective emission temperature is determined from the high-energy part of the spectrum, overestimate the low-energy part of the VAD-KEDs. This observation indicates that a purely classical model is insufficient to describe thermionic emission from the molecules under study here, and quantum effects need to be taken into account for the lowest kinetic energies. This is not surprising since the large de Broglie wavelength at low energies (123 Å at 10 meV) strongly suggests corrections to models based on classical trajectories—the great success of Vogt−Wannier/Langevin theory notwithstanding. The deviation from the classical models is particularly severe for nitropropane at excitation energies 2573 and 2922 cm^{-1}. Both of these data sets show high exponents $\gamma \approx 0.5$ in the modified Langevin model, making them very close to a pure Langevin case. We

DOI: 10.1021/acs.jpca.9b07780
J. Phys. Chem. A 2019, 123, 8562−8570

Table 2. Model Parameters for the Fits to the Experimental Data[a]

molecule	excitation wavenumber	γ^b	$T_\gamma{}^a$ (K)	$T_\mu{}^c$ (K)	$T_{\mu c}{}^c$ (K)
nitroethane	2752	0.35 ± 0.01	410 ± 7	458 ± 20	453 ± 20
	2842	0.24 ± 0.01	434 ± 10	453 ± 20	441 ± 20
	2890	0.20 ± 0.01	474 ± 12	447 ± 20	453 ± 20
	2940	0.20 ± 0.01	488 ± 10	476 ± 20	453 ± 20
nitropropane	2753	0.52 ± 0.01	288 ± 3	348 ± 20	331 ± 20
	2922	0.51 ± 0.01	298 ± 4	354 ± 20	371 ± 20
	2946	0.37 ± 0.01	309 ± 4	366 ± 20	354 ± 20
nitrobutane	2757	0.36 ± 0.01	246 ± 3	290 ± 20	290 ± 20

[a]The fit parameters of the modified Langevin model are γ and T_γ, the fitted temperatures for the point dipole and finite size dipole model are T_μ and $T_{\mu c}$, respectively. [b]Error bars are obtained from the from the nonlinear fit. [c]Error bars are 1-σ estimates.

note that the dipole moment of the molecule upon vibrational excitation will have corrections relative to the value in the vibrational ground state. We will return to this point in the discussion of the variation of the parameter γ for different vibrational excitations (see below).

Overall, the fitting results are consistent with the data, and the modified Langevin fits are in line with the expectations for the fit parameters. The neutral molecule temperature T_γ fitted with the modified Langevin cross section, given by eq 5, increases with increasing excitation energy, and it decreases for the lowest energy CH stretching excitation (i.e., for comparable vibrational modes and excitation energies) with increasing molecule size (see Table 2). The molecules have similar electron binding energies, and absorbed similar photon energies, so this behavior can be expected, since for larger molecules the energy remaining after electron emission will be distributed over a larger number of available soft vibrational modes. Using the temperatures obtained by the modified Langevin model together with the vibrational spectra of the molecules under study[37,40,67] and the statistical expression for the average internal energy of a molecule at temperature T

$$\langle U_{\mathrm{vib}}\rangle = \sum_j \frac{h\nu_j}{e^{h\nu_j/k_B T} - 1} \tag{18}$$

we find that upon excitation of the lowest energy CH stretching mode and subsequent electron emission nitroethane, nitropropane, and nitrobutane contain ca. 107, 97, and 100 meV internal vibrational energy, respectively. For the finite size dipole model, the size evolution of $T_{\mu c}$ with increasing molecule size behaves qualitatively as expected, again decreasing with increasing molecular size (see Table 2). The photon energy dependence seems significantly weaker, though.

The exponent γ in the modified Langevin model is consistent with the range expected for the model (between 0 and 0.5), which reflects the idea that the capture cross section should fall off more quickly than $E^{-1/2}$, in other words, faster than the Wigner threshold law for *s*-wave capture but slower than the de Broglie cross section ($\propto 1/E$).

Figures 4 and 5 show the VAD-KEDs for various excitation energies in nitroethane and nitropropane, respectively. The excited vibrational modes were chosen based on their intensity and how well resolved they are in the electron loss spectra of the molecules.[25] The electron loss spectrum for nitrobutane was judged to be too congested to resolve individual vibrational excited states except for the lowest energy CH stretching mode. For nitroethane, the higher energy VAD-KEDs show slightly more structure than those at the lowest excitation energies, in particular a somewhat more pronounced

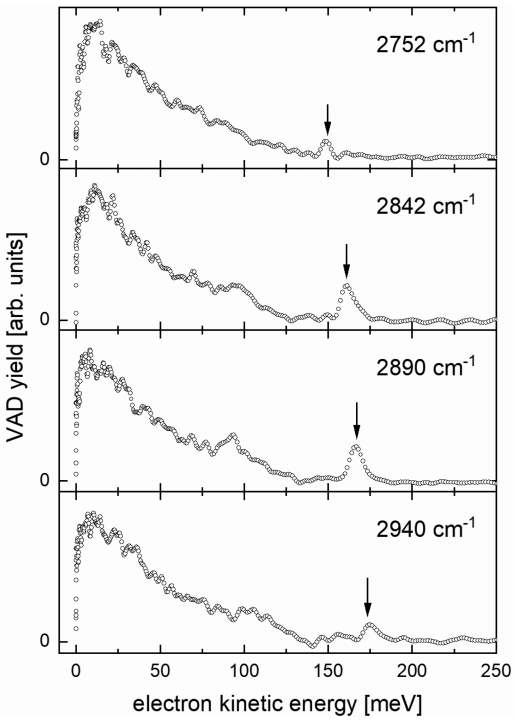

Figure 4. Mode dependence of the VAD-KEDs for nitroethane. The excitation wavenumbers are noted in each panel. From top to bottom, the vibrational excited states[25] are ν_5 (stretch of the CH group *syn* to the NO_2 group); ν_4 (CH_3 symmetric stretch); strongly mixed overtones and combination bands of the methyl bending mode ν_8; and the close-lying levels ν_3 (methylene stretching) and $2\nu_6$ (HCH bending). The parameters for various models are listed in Table 2.

0 → 0 band and a shoulder around electron kinetic energies of 100 meV (ca. 75 meV lower than the 0 → 0 feature), which can be identified as signatures of the 0 → 1 transition in the nitro wagging mode.[39] For nitropropane, we observe a broad feature at ca. 80 meV kinetic energy, which is consistent with the 0 → 1 transition of the nitro wagging mode,[37] even though the large width and the apparent absence of the 0 → 0 transition make this assignment less firm. These features suggest that the intramolecular vibrational relaxation process is energy- or even mode-specific, a phenomenon which has been observed much more clearly in nitromethane.[6] As low-lying final states seem to increase in intensity relative to the purely thermal VAD-KEDs, this energy or mode specificity leads to a slightly broader envelope of the VAD-KEDs, which in turn results in slightly smaller γ values in the fits to the modified Langevin model. However, the change in γ is only 0.01−0.02

DOI: 10.1021/acs.jpca.9b07780
J. Phys. Chem. A 2019, 123, 8562−8570

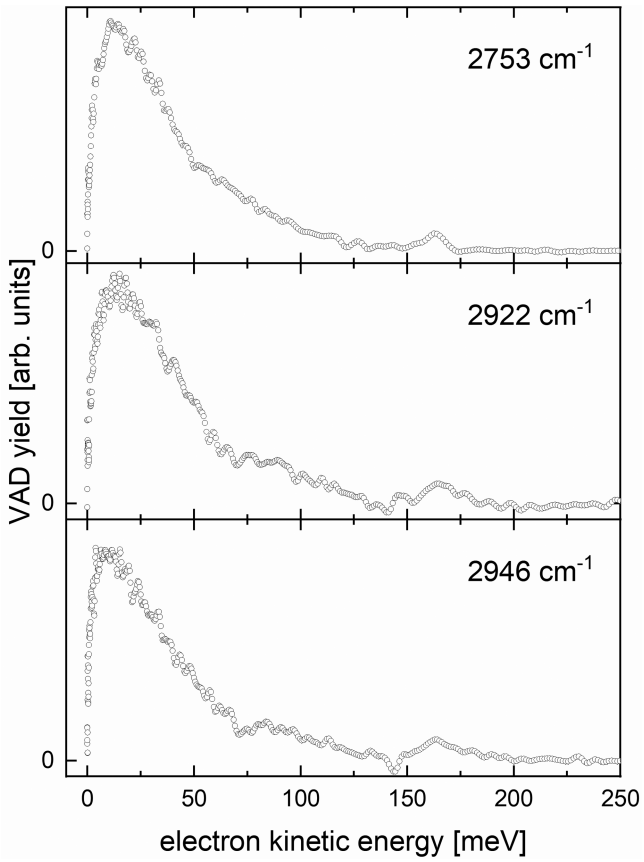

Figure 5. Mode dependence of the VAD-KEDs for nitropropane. The excitation wavenumbers are noted in each panel. The parameters for various models are listed in Table 2. The large number of Fermi interactions in the CH stretching region and the complexity of the spectrum of nitropropane anion prevent us from a more detailed mode assignment.

compared to a fit where the data range was restricted to lower kinetic energies, excluding the features in question. The clear changes of the γ values at higher excitation energies from those at the lowest energies are therefore clearly not artifacts of the fit.

The actual values for γ depend not only on the molecule but also on the initially excited vibration, and the temperatures T_γ increase with increasing excitation energy. The temperatures T_μ and $T_{\mu c}$ for the classical dipole model also vary for different initially excited vibrations, although there is no clear trend. The temperature dependence as observed for the modified Langevin model can be qualitatively understood, since a higher final temperature of the neutral product molecule is expected for a higher excitation energy. The temperature increase for nitroethane is somewhat higher than expected from the range of photon energies used. The reason for the variation of γ values is not *a priori* clear but may be connected to this observation. We note, however, that the parametrization in terms of the single parameter γ will not necessarily reproduce both the dependence on the kinetic energy of the emitted electron and on the excitation energy. Another possible explanation for the mode specific behavior of γ invokes a mode specific path through vibrational state space offered by different initial excited states. If the vibrational state at the time of electron emission depends on the initially excited state, the average effective dipole moment of the remaining neutral molecule can also depend on the initially excited state. This results in a different field in which the outgoing electron moves, affecting the dependence of the thermionic emission process on the electron kinetic energy. If this hypothesis is correct, it implies that energy randomization is not complete. The different intensities of the $0 \rightarrow 0$ bands in the VAD-KEDs are consistent with this explanation, although we do not consider them as proof for this hypothesis. In any case, it should be kept in mind that the bulk parts of the KEDs are composed of the smooth distributions that point to statistical processes.

5. CONCLUSIONS

We have presented experimental results on the kinetic energy distributions of vibrational autodetachment in negatively charged nitroalkane molecules. While the VAD-KED of nitromethane shows very pronounced vibrational structure, nitroethane, 1-nitropropane, and 1-nitrobutane exhibit rather smooth VAD-KEDs. It is striking that already the addition of even a single CH_2 group to nitromethane (i.e., going to nitroethane) results in a behavior that lends itself to a statistical description, where molecular details such as the vibrational spectrum of the molecule only play a small role. We were able to describe the observed VAD-KEDs with a thermionic emission model based on a detailed balance approach. The electron capture cross section used in this model can be described classically as well as with an empirical ansatz rooted in limiting quantum mechanical behavior. The latter model gives an excellent description of the kinetic energy distributions for all kinetic energies, better than the purely classical cross sections, but all models used here are in good agreement with the experimental data at energies above 20 meV. An increase in excitation energy or a decrease in molecular size results in a higher microcanonical temperature of the neutral molecule that remains behind after electron emission.

■ ASSOCIATED CONTENT

Supporting Information

The Supporting Information is available free of charge on the ACS Publications website at DOI: 10.1021/acs.jpca.9b07780.

Additional classical point dipole and modified Langevin fits to all excitation energies (see Table 2) (PDF)

■ AUTHOR INFORMATION

Corresponding Authors

*E-mail: weberjm@jila.colorado.edu.

*E-mail: klavshansen@tju.edu.cn.

ORCID

Klavs Hansen: 0000-0001-9746-3711

J. Mathias Weber: 0000-0002-5493-5886

Present Address

C.L.A.: Adams State University, 208 Edgemont Blvd., Alamosa, CO 81101.

Notes

The authors declare no competing financial interest.

■ ACKNOWLEDGMENTS

We gratefully acknowledge funding from the National Science Foundation (NSF) through the NSF AMO Physics Frontier Center at JILA (PHY-1734006).

DOI: 10.1021/acs.jpca.9b07780
J. Phys. Chem. A 2019, 123, 8562−8570

REFERENCES

(1) Richardson, O. W. *The Emission of Electricity from Hot Bodies*; Longmans Green and Company: London, 1921.

(2) Weidele, H.; Kreisle, D.; Recknagel, E.; Schulze-Icking-Konert, G.; Handschuh, H.; Ganteför, G.; Eberhardt, W. Thermionic Emission from Small Clusters - Direct Observation of the Kinetic-Energy Distribution of the Electrons. *Chem. Phys. Lett.* **1995**, *237*, 425−431.

(3) Wurz, P.; Lykke, K. R. Delayed Electron-Emission from Photoexcited C_{60}. *J. Chem. Phys.* **1991**, *95*, 7008−7012.

(4) Campbell, E. E. B.; Ulmer, G.; Hertel, I. V. Delayed Ionization of C_{60} and C_{70}. *Phys. Rev. Lett.* **1991**, *67*, 1986−1988.

(5) Andersen, J. U.; Bonderup, E.; Hansen, K. Thermionic Emission from Clusters. *J. Phys. B: At. Mol. Opt. Phys.* **2002**, *35*, R1−R30.

(6) Adams, C. L.; Schneider, H.; Weber, J. M. Vibrational Autodetachment − Intramolecular Vibrational Relaxation Translated into Electronic Motion. *J. Phys. Chem. A* **2010**, *114*, 4017−4030.

(7) Simons, J. Propensity Rules for Vibration-Induced Electron Detachment of Anions. *J. Am. Chem. Soc.* **1981**, *103*, 3971−3976.

(8) Ebara, Y.; Furukawa, T.; Matsumoto, J.; Tanuma, H.; Azuma, T.; Shiromaru, H.; Hansen, K. Detection of Recurrent Fluorescence Photons. *Phys. Rev. Lett.* **2016**, *117*, 133004.

(9) Acharya, P. K.; Kendall, R. A.; Simons, J. Vibration-Induced Electron Detachment in Molecular Anions. *J. Am. Chem. Soc.* **1984**, *106*, 3402−3407.

(10) Meyer, F. K.; Jasinski, J. M.; Rosenfeld, R. N.; Brauman, J. I. Infrared Multi-Photon Photodetachment of Negative-Ions in the Gas-Phase. *J. Am. Chem. Soc.* **1982**, *104*, 663−667.

(11) Rosenfeld, R. N.; Jasinski, J. M.; Brauman, J. I. Infrared Multi-Photon Electron Detachment from the Benzyl Anion. *J. Chem. Phys.* **1979**, *71*, 1030−1031.

(12) Foster, R. F.; Tumas, W.; Brauman, J. I. Unimolecular Decomposition and Vibrationally Induced Electron Autodetachment of Acetone Enolate Ion. *J. Chem. Phys.* **1983**, *79*, 4644−4646.

(13) Tumas, W.; Salomon, K. E.; Brauman, J. I. Dimethylsilanone Enolate Anion - Competitive Fragmentation and Electron Autodetachment of Vibrationally Excited Siloxide Anions in the Gas-Phase. *J. Am. Chem. Soc.* **1986**, *108*, 2541−2546.

(14) Wight, C. A.; Beauchamp, J. L. Infrared-Spectra of Gas-Phase Ions and Their Use in Elucidating Reaction-Mechanisms - Identification of C_7H_7-Structural Isomers by Multi-Photon Electron Detachment Using a Low-Power Infrared-Laser. *J. Am. Chem. Soc.* **1981**, *103*, 6499−6501.

(15) Wight, C. A.; Beauchamp, J. L. Multiphoton Electron Detachment Studies of $C_7H_7^-$ Using a Low-Power Infrared-Laser - Competition of Radiative and Collisional Relaxation with Vibrational-Excitation. *Chem. Phys.* **1989**, *134*, 375−384.

(16) Wight, C. A.; Beauchamp, J. L. Infrared-Spectra of Butenyl Anions - Multiphoton Electron Detachment as a Photochemical Probe of Isomeric Structures of Gas-Phase Anions. *Int. J. Mass Spectrom. Ion Processes* **1990**, *100*, 445−455.

(17) Neumark, D. M.; Lykke, K. R.; Andersen, T.; Lineberger, W. C. Infrared-Spectrum and Autodetachment Dynamics of NH^-. *J. Chem. Phys.* **1985**, *83*, 4364−4373.

(18) Mullin, A. S.; Murray, K. K.; Schulz, C. P.; Szaflarski, D. M.; Lineberger, W. C. Autodetachment Spectroscopy of Vibrationally Excited Acetaldehyde Enolate Anion, CH_2CHO. *Chem. Phys.* **1992**, *166*, 207−213.

(19) Weber, J. M.; Robertson, W. H.; Johnson, M. A. Argon Predissociation and Electron Autodetachment Spectroscopy of Size-Selected $CH_3NO_2^-\cdot Ar_n$ Clusters. *J. Chem. Phys.* **2001**, *115*, 10718−10723.

(20) Elliott, B. M.; McCunn, L. R.; Johnson, M. A. Photoelectron Imaging Study of Vibrationally Mediated Electron Autodetachment in the Type I Isomer of the Water Hexamer Anion. *Chem. Phys. Lett.* **2008**, *467*, 32−36.

(21) DeVine, J. A.; Weichman, M. L.; Xie, C. J.; Babin, M. C.; Johnson, M. A.; Ma, J. Y.; Guo, H.; Neumark, D. M. Autodetachment from Vibrationally Excited Vinylidene Anions. *J. Phys. Chem. Lett.* **2018**, *9*, 1058−1063.

(22) Henley, A.; Fielding, H. H. Anion Photoelectron Spectroscopy of Protein Chromophores. *Int. Rev. Phys. Chem.* **2019**, *38*, 1−34.

(23) Parkes, M. A.; Bennett, A.; Fielding, H. H. A Photoelectron Imaging and Quantum Chemistry Study of the Deprotonated Cyan Fluorescent Protein Chromophore Anion. *Mol. Phys.* **2019**, 1.

(24) Saha, K.; Prabhakaran, A.; Chandrasekaran, V.; Rappaport, M. L.; Heber, O.; Zajfman, D. An Experimental Setup to Study Delayed Electron Emission Upon Photoexcitation of Trapped Polyatomic Anions. *Rev. Sci. Instrum.* **2017**, *88*, 053101.

(25) Schneider, H.; Vogelhuber, K. M.; Schinle, F.; Stanton, J. F.; Weber, J. M. Vibrational Spectroscopy of Nitroalkane Chains Using Electron Detachment and Ar Predissociation. *J. Phys. Chem. A* **2008**, *112*, 7498−7506.

(26) Knurr, B. J.; Adams, C. L.; Weber, J. M. Infrared Spectroscopy of Hydrated Naphthalene Cluster Anions. *J. Chem. Phys.* **2012**, *137*, 104303.

(27) Thompson, M. C.; Baraban, J. H.; Matthews, D. A.; Stanton, J. F.; Weber, J. M. Heavy Atom Vibrational Modes and Low-Energy Vibrational Autodetachment in Nitromethane Anions. *J. Chem. Phys.* **2015**, *142*, 234304.

(28) Liu, H. T.; Ning, C. G.; Huang, D. L.; Dau, P. D.; Wang, L. S. Observation of Mode-Specific Vibrational Autodetachment from Dipole-Bound States of Cold Anions. *Angew. Chem., Int. Ed.* **2013**, *52*, 8976−8979.

(29) Liu, H. T.; Ning, C. G.; Huang, D. L.; Wang, L. S. Vibrational Spectroscopy of the Dehydrogenated Uracil Radical by Autodetachment of Dipole-Bound Excited States of Cold Anions. *Angew. Chem., Int. Ed.* **2014**, *53*, 2464−2468.

(30) Regeta, K.; Allan, M. Autodetachment Dynamics of Acrylonitrile Anion Revealed by Two-Dimensional Electron Impact Spectra. *Phys. Rev. Lett.* **2013**, *110*, 203201.

(31) Yandell, M. A.; King, S. B.; Neumark, D. M. Decay Dynamics of Nascent Acetonitrile and Nitromethane Dipole-Bound Anions Produced by Intracluster Charge-Transfer. *J. Chem. Phys.* **2014**, *140*, 184317.

(32) Steill, J. D.; Oomens, J. Spectroscopically Resolved Competition between Dissociation and Detachment from Nitrobenzene Radical Anion. *Int. J. Mass Spectrom.* **2011**, *308*, 239−252.

(33) Bull, J. N.; West, C. W.; Verlet, J. R. R. Ultrafast Dynamics of Formation and Autodetachment of a Dipole-Bound State in an Open-Shell Π-Stacked Dimer Anion. *Chemical Science* **2016**, *7*, 5352−5361.

(34) Bull, J. N.; Verlet, J. R. R. Observation and Ultrafast Dynamics of a Nonvalence Correlation-Bound State of an Anion. *Sci. Adv.* **2017**, *3*, No. e1603106.

(35) Hansen, K.; Echt, O. Thermionic Emission and Fragmentation of C_{60}. *Phys. Rev. Lett.* **1997**, *78*, 2337−2340.

(36) Yeretzian, C.; Hansen, K.; Whetten, R. L. Rates of Electron-Emission from Negatively Charged, Impact-Heated Fullerenes. *Science* **1993**, *260*, 652−656.

(37) Adams, C. L.; Knurr, B. J.; Weber, J. M. Photoelectron Spectroscopy of 1-Nitropropane and 1-Nitrobutane Anions. *J. Chem. Phys.* **2012**, *136*, 064307.

(38) Adams, C. L.; Schneider, H.; Ervin, K. M.; Weber, J. M. Low-Energy Photoelectron Imaging Spectroscopy of Nitromethane Anions: Electron Affinity, Vibrational Features, Anisotropies and the Dipole-Bound State. *J. Chem. Phys.* **2009**, *130*, 074307.

(39) Adams, C. L.; Weber, J. M. Photoelectron Imaging Spectroscopy of Nitroethane Anions. *J. Chem. Phys.* **2011**, *134*, 244301.

(40) Groner, P.; Meyer, R.; Günter, A.; Kühne, H.; Günthard, H. H. Far Infrared-Spectrum of Nitroethane. *Chem. Phys.* **1974**, *5*, 136−141.

(41) Lide, D. R. *CRC Handbook of Chemistry and Physics*, 86th ed.; Taylor & Francis Group: Boca Raton, FL, 2005.

(42) Miller, J. G.; Angel, H. S. The Dipole Moment of 1-Nitrobutane. *J. Am. Chem. Soc.* **1946**, *68*, 2358−2359.

(43) Li, W.; Chambreau, S. D.; Lahankar, S. A.; Suits, A. G. Megapixel Ion Imaging with Standard Video. *Rev. Sci. Instrum.* **2005**, *76*, 063106.

DOI: 10.1021/acs.jpca.9b07780
J. Phys. Chem. A 2019, 123, 8562−8570

(44) Dribinski, V.; Ossadtchi, A.; Mandelshtam, V. A.; Reisler, H. Reconstruction of Abel-Transformable Images: The Gaussian Basis-Set Expansion Abel Transform Method. *Rev. Sci. Instrum.* **2002**, *73*, 2634−2642.
(45) Weisskopf, V. Statistics and Nuclear Reactions. *Phys. Rev.* **1937**, *52*, 295−303.
(46) Andersen, J. U.; Bonderup, E.; Hansen, K. On the Concept of Temperature for a Small Isolated System. *J. Chem. Phys.* **2001**, *114*, 6518−6525.
(47) Bethe, H. A. Theory of Disintegration of Nuclei by Neutrons. *Phys. Rev.* **1935**, *47*, 747−759.
(48) Wigner, E. P. On the Behavior of Cross Sections near Thresholds. *Phys. Rev.* **1948**, *73*, 1002−1009.
(49) Fabrikant, II; Hotop, H. Low-Energy Behavior of Exothermic Dissociative Electron Attachment. *Phys. Rev. A: At., Mol., Opt. Phys.* **2001**, *63*, 022706.
(50) Hotop, H.; Ruf, M. W.; Allan, M.; Fabrikant. Resonance and Threshold Phenomena in Low-Energy Electron Collisions with Molecules and Clusters. *Adv. At., Mol., Opt. Phys.* **2003**, *49*, 85−216.
(51) Hotop, H.; Ruf, M. W.; Fabrikant, I. I. Resonance and Threshold Phenomena in Low-Energy Electron Collisions with Molecules and Clusters. *Phys. Scr.* **2004**, *110*, 22−31.
(52) Barsotti, S.; Fabrikant, II; Ruf, M. W.; Hotop, H. High Resolution Low-Energy Electron Attachment to Molecular Clusters of Sulfur Dioxide. *Int. J. Mass Spectrom.* **2014**, *365*, 301−310.
(53) Kopyra, J.; Szamrej, I.; Graupner, K.; Graham, L. M.; Field, T. A.; Sulzer, P.; Denifl, S.; Mark, T. D.; Scheier, P.; Fabrikant, II; Braun, M.; Ruf, M. W.; Hotop, H. Low-Energy Electron Attachment to Chloroform (Chcl3) Molecules: A Joint Experimental and Theoretical Study. *Int. J. Mass Spectrom.* **2008**, *277*, 130−141.
(54) Braun, M.; Fabrikant, II; Ruf, M. W.; Hotop, H. Low-Energy Electron Collisions with CH_3Br: The Dependence of Elastic Scattering, Vibrational Excitation, and Dissociative Attachment on the Initial Vibrational Energy. *J. Phys. B: At., Mol. Opt. Phys.* **2007**, *40*, 659−674.
(55) Marienfeld, S.; Sunagawa, T.; Fabrikant, II; Braun, M.; Ruf, M. W.; Hotop, H. The Dependence of Low-Energy Electron Attachment to CF_3Br on Electron and Vibrational Energy. *J. Chem. Phys.* **2006**, *124*, 154316.
(56) Klar, D.; Ruf, M. W.; Hotop, H. Attachment of Electrons to Molecules at meV Resolution. *Aust. J. Phys.* **1992**, *45*, 263−291.
(57) Klar, D.; Ruf, M. W.; Hotop, H. Attachment of Electrons to Molecules at Submillielectronvolt Resolution. *Chem. Phys. Lett.* **1992**, *189*, 448−454.
(58) Fermi, E.; Teller, E. The Capture of Negative Mesotrons in Matter. *Phys. Rev.* **1947**, *72*, 399−408.
(59) Desfrancois, C.; Abdoul-Carime, H.; Khelifa, N.; Schermann, J. P. From 1/R to 1/R(2) Potentials - Electron-Exchange between Rydberg Atoms and Polar-Molecules. *Phys. Rev. Lett.* **1994**, *73*, 2436−2439.
(60) Dashevskaya, E. I.; Litvin, I.; Nikitin, E. E.; Troe, J. Quantum and Classical Fall of a Charged Particle onto a Stationary Dipolar Target. *J. Phys. Chem. A* **2009**, *113*, 14212−14219.
(61) Dashevskaya, E. I.; Litvin, I.; Nikitin, E. E.; Troe, J. Electron Capture by Polarizable Dipolar Targets: Numerical and Analytically Approximated Capture Probabilities. *J. Phys. Chem. A* **2011**, *115*, 6825−6830.
(62) Klots, C. E. Rate Constants for Unimolecular Decomposition at Threshold. *Chem. Phys. Lett.* **1976**, *38*, 61−64.
(63) Langevin, P. A. Fundamental Formula of Kinetic Theory. *Ann. Chim. Phys.* **1905**, *5*, 245−288.
(64) Vogt, E.; Wannier, G. H. Scattering of Ions by Polarization Forces. *Phys. Rev.* **1954**, *95*, 1190−1198.
(65) Hansen, K. The Classical Capture Cross Section of an Electron and Neutral and Anionic Polarizable Molecules with Permanent Dipole Moments. *Int. J. Mass Spectrom.* **2019**, *438*, 142−147.
(66) Marcum, J. C.; Weber, J. M. Microhydration of Nitromethane Anions from Both a Solute and Solvent Perspective. *J. Phys. Chem. A* **2010**, *114*, 8933−8938.
(67) Shilina, M. I.; Senyavin, V. M.; Kuramshina, G. M.; Smirnov, V. V.; Pentin, Y. A. Vibrational Spectra, Assignment, Conformational Stability and Ab Initio/DFT Calculations for 1-Nitropropane. *Struct. Chem.* **2003**, *14*, 559−573.

DOI: 10.1021/acs.jpca.9b07780
J. Phys. Chem. A 2019, 123, 8562−8570